Inter-backbone charge transfer as prerequisite for long-range conductivity in perylenebisimide hydrogels

Max Burian[1,$], Francesco Rigodanza[2,$], Nicola Demitri[3], Silvia Marchesan[2], Tereza Steinhartova[4,5], Ilse Letofsky-Papst[6], Ivan Khalakhan[7], Eléonore Mourad[8], Stefan A. Freunberger[8], Heinz Amenitsch[1*], Maurizio Prato[2,9,10*], and Zois Syrgiannis[2*]

[1] Institute of Inorganic Chemistry, Graz University of Technology, Stremayrgasse 9/IV, 8010 Graz, Austria.

[2] Center of Excellence for Nanostructured Materials (CENMAT) and INSTM, unit of Trieste, Department of Chemical and Pharmaceutical Sciences, University of Trieste, via L. Giorgieri 1, 34127 Trieste, Italy.

[3] Elettra-Sincrotrone Trieste, Strada Statale 14, km 163.5 in AREA Science Park, 34149 Basovizza, Trieste, Italy.

[4] Istituto Officina dei Materiali, IOM – CNR, SS. 14 km 163.5 in Area Science Park, 34149 Basovizza, Italy.

[5] Department of Physics, University of Trieste, 34128 Trieste, Italy.

[6] Institute for Electron Microscopy & Nanoanalysis and Center for Electron Microscopy, Graz University of Technology, NAWI Graz, Steyrergasse 17, 8010 Graz, Austria.

[7] Department of Surface and Plasma Science, Faculty of Mathematics and Physics, Charles University, V Holešovičkách 2, 180 00 Praha 8, Czech Republic.

[8] Institute for Chemistry and Technology of Materials, Graz University of Technology, Stremayrgasse 9, 8010 Graz, Austria.

[9] Carbon Nanobiotechnology Laboratory CIC biomaGUNE, Paseo de Miramón 182 20009 Donostia-San Sebastian, Spain;

[10] Basque Fdn Sci, Ikerbasque, Bilbao 48013, Spain.

[*] Correspondence should be addressed to Z.S. (email: zsyrgiannis@units.it) or to M.P. (email: prato@units.it) or to H.A. (email: amenitsch@tugraz.at)

[$] These authors contributed equally to this work.

Hydrogelation, the self-assembly of molecules into soft, water-loaded networks, bridges the structural gap between single molecules and functional materials. The potential of hydrogels, such as those based on perylenes, lies in their chemical, physical, optical, and electronic properties, which are all governed by the inter- and supramolecular structure of the gel. However, this structural motif and its precise role for long-range conductivity are unknown. Here, we present a comprehensive structural picture of a perylenebisimide hydrogel, suggesting that its long-range conductivity is limited by charge-transfer between electronic backbones. We reveal nano-crystalline ribbons as the electronic and structural backbone between which charge transfer is mediated by polar solvent bridges. We exemplify this effect with gas sensing, where exposure to polar vapour changes conductivity by five orders of magnitude, emphasising the crucial role of the interplay between structural motif and surrounding medium for the rational design of devices based on nano-crystalline hydrogels.

Organic semiconductors based on perylene bisimide (PBI) dyes have gained enormous attention due to their manifold potential applications. PBIs are robust organic molecules characterized of (i) a broad visible absorption cross-section, (ii) low cost of the sustainable metal-free raw materials, (iii) high thermal, photo, and oxidative stability and (iv) versatile ways to tune stereo-electronic properties of the photo-responsive core[1, 2]. The aromatic π-conjugated PBI core is not only responsible for the molecule's optical properties but also for its tendency to self-assemble through π-π-interactions[3], leading to highly-ordered supramolecular aggregates that find application in water-splitting, organic field-effect transistors and sensors[4, 5, 6, 7, 8, 9]. However, the molecular arrangement not only induces a structural motif, but also affects the molecular dipole-dipole alignments and therefore the electronic and optical properties[10, 11, 12, 13]. According to this structure-function correlation, a clear and precise characterization of PBI based materials on the molecular level is inevitable for the design of future devices.

Due to its hydrophobic nature, the structure defining π-π-interaction is particularly strong in aqueous solvents – a principle that can be used to form water-based soft, molecular networks called hydrogels[14, 15]. Hydrogels find their full potential within their hierarchical nature: At the macroscopic level, hydrogels are highly porous materials that are easily loaded with, e.g., colloidal nanocatalysts and allow diffusion of educts and products to the reaction sites[16, 17, 18, 19, 20]. On the molecular level, perylene based gels consist of π-π-stacked structures, capable of charge-separation and transport[21, 22, 23, 24]. While this molecular motif is thought to act as the electronic and structural backbone of the gel[23], the long-range charge-transfer mechanism *between* these backbones, a prerequisite for application, is unknown.

Herein, we present a comprehensive structural framework of the pH-triggered hydrogel using single crystal diffraction, mechanical, spectroscopic, scattering and imaging techniques and we provide evidence for solvent-mediated inter-backbone charge transfer in PBI hydrogels. We reconstruct the underlying structural motif over a wide length-scale ranging from crystalline nano-ribbons, which act as the electronic and structural backbone, to their macroscopic arrangement. We find macroscopic conductivity of the dried gel only in the presence of a polar vapour, revealing the importance of inter-backbone hydrogen-bonding as charge-transfer bridges. We use this effect in gas-sensing devices that change electronic conductivity by five orders of magnitude within milliseconds in response to polar vapour concentration. The awareness of this inter-backbone charge-transfer mechanism is not only crucial to understand and design PBI based hydrogels but also to exploit the full potential of chemically related nano-crystalline hydrogel based devices.

The precursor. We synthesized N,N'-bis(propanoic acid)-perylene-3,4,9,10-tetracarboxylic bisimide (**PBI1 -** Fig. 1a) using a microwave assisted protocol (see Supplementary Information for details)[25] and prepared a 8.8 mM **PBI1** precursor in basic (pH 10) trimethylamine (TEA) in H_2O solution. To understand the molecular interactions of **PBI1** under these conditions, we

obtained crystallographic data of single crystals grown from the precursor (for details see single crystal analysis in the Supplementary Information).In its single-crystalline form, **PBI1** forms typical π-π-stacked columns (nanorods)[26] as shown in Fig. 1b and Supplementary Fig. 1. Within these columns, the molecules are both longitudinally and transversally shifted such that the stacking direction is tilted by 23° away from the direction perpendicular to the perylene plane (Fig. 1b). The tilted axis is most likely caused by intra-columnar hydrogen-bonding between the carboxylic groups, resulting in sandwiched **PBI1**-trimers (yellow circle in Fig. 1b and Supplementary Fig. 1). This motif leaves two unused carboxylic-moieties per triplet, which offer binding sites that allow cross-linking between longitudinal neighbouring columns (blue circle in Fig. 1b). In addition, the hydrophobic interaction of the perylene core causes transversal attraction between the stacks to minimize the core's exposure to the polar medium. This single-crystalline motif, in particular the columnar arrangement of **PBI1**, is the structural cornerstone for the following sections.

Gel formation and characterization. Acidifying the basic precursor solution of **PBI1** with 4 M HCl to pH 4 commences the gelation process. After an aging period of approx. 4 min, the liquid precursor transforms into a gel-like substance that it is capable of holding its own weight in a glass vial (see Supplementary Fig. 2a and Synthesis in the Supplementary Information for further details). Oscillatory rheometry analysis of the gelification process shows an increase in storage modulus G' from 0.7 to 1.4 kPa and loss modulus G'' from 0.10 to 0.12 kPa within minutes after mixing (Supplementary Fig. 2b). Differential Scanning Calorimetry (DSC) of the final gel reveals a remarkably high gel-to-sol transition temperature with an onset at 83.7 ± 1.0 °C, and an endothermal peak, corresponding to the melting temperature T_m, at 91.9 °C $\pm$ 1.1 °C (Supplementary Fig. 2e).

Gelation changes the sample colour from dark red to black/dark brown (Supplementary Fig. 2a). This colour change suggests a change in molecular structure and electronic states in

accord with the general structure-function relation in molecular photodyes such as **PBI1**[23]. To understand this transition, we investigated the optical and structural nature of precursor and hydrogel by means of UV/Vis absorption, small angle-x-ray scattering (SAXS) and cryogenic transmission electron microscopy (CryoTEM) (Fig. 1c–e).
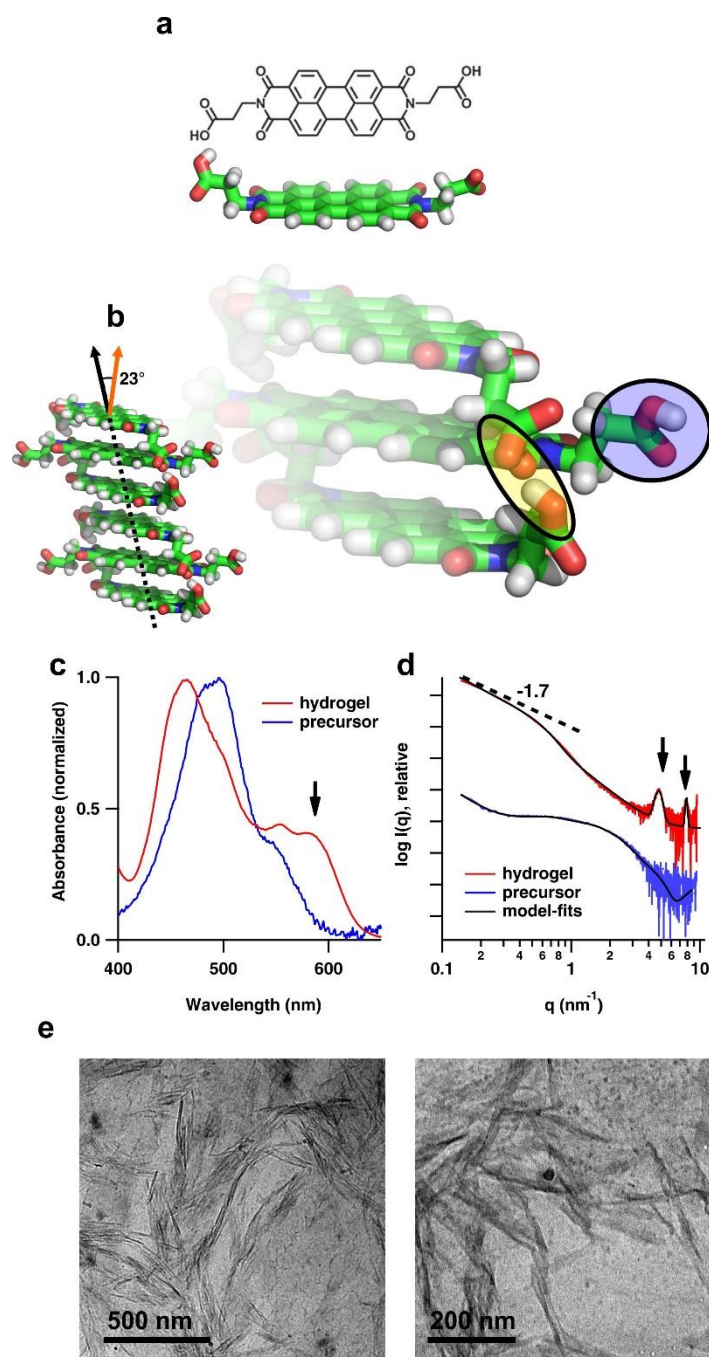

Figure 1| Structural characterization of PBI1 on the nanometer scale. a, Representation and graphical model of the **PBI1** molecule. **b**, Molecular model of the π-π-stacked columns found in the crystal structure, illustrating the 23° difference between column axis (black arrow) and the direction perpendicular to the **PBI1** core (orange arrow). The magnified view highlights the intra-columnar hydrogen bonding between carboxylic groups within

the characteristic **PBI1** triplet (yellow circle), leaving one sandwiched carboxylic group unbound (blue circle). **c,** UV/Vis absorption spectra of the **PBI1** precursor solution before addition of HCl (blue) and in the hydrogel (red) state. The black arrow indicates the absorption peak characteristic for *J*-type aggregation in the hydrogel. **d,** SAXS patterns corresponding to the UV/Vis absorption measurements in **c**, together with with the full-pattern refined model-fits (black). The two black arrows indicate the positions of Bragg-peaks, characteristic for the nano-crystalline nature of the hydrogel. **e,** Two representative CryoTEM images of the hydrogel clearly reveal a ribbon-like structure.

Generally, perylene bisimides exhibit a fine vibronic structure of the main electronic transitions S1 ← S0.[27] Yet, molecular aggregation strongly affects the optical bands due to excitonic interactions between neighbouring chromophores[27]. The precursor solution exhibits a strong dimeric band at 500 nm, whereas only a shoulder at 554 nm hints at the position of the monomeric S1 ← S0 band (Fig. 1c, blue trace and Supplementary Fig. 5 for peak-fit). Such a suppression has been shown to result from *H*-type aggregation via π-π-stacking, indicating perpendicular stacking to the parallel **PBI1** cores. Gelation of the precursor caused a general broadening of the absorption spectrum due to enhanced electronic coupling between chromophores (Fig. 1c, red trace and Supplementary Fig. 3 for peak-fit) [28, 29, 30]. Further, the H-dimeric peak strongly blue-shifts by 30 nm from 500 nm to 462 nm while the monomeric peak remains at 554 nm. Most interestingly, a new peak at 588 nm arises as indicated by the black arrow in Fig. 1c – a behaviour that has previously been linked to *J*-type aggregation through π-π-interactions[31]. Thus, UV-Vis suggests the gelation process to cause a *H*- to *J*-type transition, possibly related to a shift of the stacking direction away from the axis perpendicular the **PBI1** molecular core[32].

To obtain more direct information on the structural motif of the **PBI1** in the precursor, the transition during gelification, and the final gel, we performed SAXS measurements. The scattering data of the protonated precursor state (basic aqueous solution) shows a low–q transition to the Guinier regime (q^{-0}), which is characteristic for form-factor scattering of non-aggregated particles (Fig. 1d). To model the pattern, we used a single **PBI1** molecule from the single-crystal structure to build a series of progressively stacked *H*-type arrays (more details

about the modelling are given in the section SAXS model fitting in the Supplementary Information). Best agreement between model and data was found for π-π-stacked tetramers (Supplementary Fig. 4), and full pattern refinement suggests 4 nm mean distance between the tetramers (Fig. 1d, black trace). Thus, the hydrophobic attraction of the perylene cores causes short column-like assemblies, in agreement with literature and the UV/Vis measurements.

We observed the structural transition from precursor to hydrogel using *in-situ* SAXS measurements during the gelation process and found two distinct phenomena (Supplementary Fig. 5a). First, the scattering intensity in the low–q regime ($1 < q < 2$ nm^{-1}) strongly increases – an indicator for a growing structural motif. Second, two diffraction peaks in the mid–q regime ($4 < q < 5$ nm^{-1}) form, which suggests crystalline ordering. The comparison of the integral intensities of the two reciprocal space regions connects these named mechanisms (Supplementary Fig. 5b). A more detailed analysis of the SAXS pattern of the hydrogel (Fig. 1d, red trace) shows as the most striking difference to the precursor the transition in the low–q region: the power-law slope has increased from q^{-0} to $q^{-1.8}$. Such a behaviour is characteristic for the presence of a two-dimensional motif, such as, e.g., sheet- or ribbon-like structures with internal disorder and porosity (q^{-2} slope in the case of a solid sheet-like structure)[33]. A Guinier fit reveals an approximate sheet thickness of 5 nm (see SAXS model fitting in the Supplementary Information for more details). Transmission electron microscopy (TEM) images taken under cryogenic conditions (CryoTEM) show a similar ribbon-like motif (Fig. 1e and Supplementary Fig. 6 for magnification) with the ribbons also acting as the structural backbone through cross-linking between them. Atomic force microscopy (AFM) images of a drop-casted sample confirm a ribbon thickness of approx. 5 nm (Supplementary Fig. 7).

The SAXS pattern of the final hydrogel shows two distinct peaks as indicated by the black arrows in Fig. 1d. These peaks are caused by a recurrent structural motif in the hydrogel and can hence be used to reverse-engineer the molecular architecture. The wide angle scattering

pattern present five strong reflections in addition to three significantly weaker ones (Fig. 2a).

Comparison of this scattering pattern with the scattering of the single-crystal grown from the precursor (see Supplementary Fig. 8) immediately identifies only one consistent structural feature: the strong peak at 18.28 nm^{-1} is indicative of the π-π-stacking distance between perylene cores within a single **PBI1** column. Other reflections seen in the single-crystal scattering are not found in the hydrogel scattering, suggesting a different arrangement of the prevailing π-π-stacked columns in the hydrogel compared to the single-crystal. Indeed, all but the latter two reflections can be indexed using a two-dimensional oblique (P1) lattice[5] with a = 2.188 nm, b = 1.367 nm, and γ = 36.14° (see indexing in Fig. 2a and for details see x-ray diffraction analysis in the Supplementary Information). The peak at 18.86 nm^{-1} following the characteristic π-π-stacking peak is most likely caused by a vertical misalignment between the π-π diffraction planes of neighbouring columns.
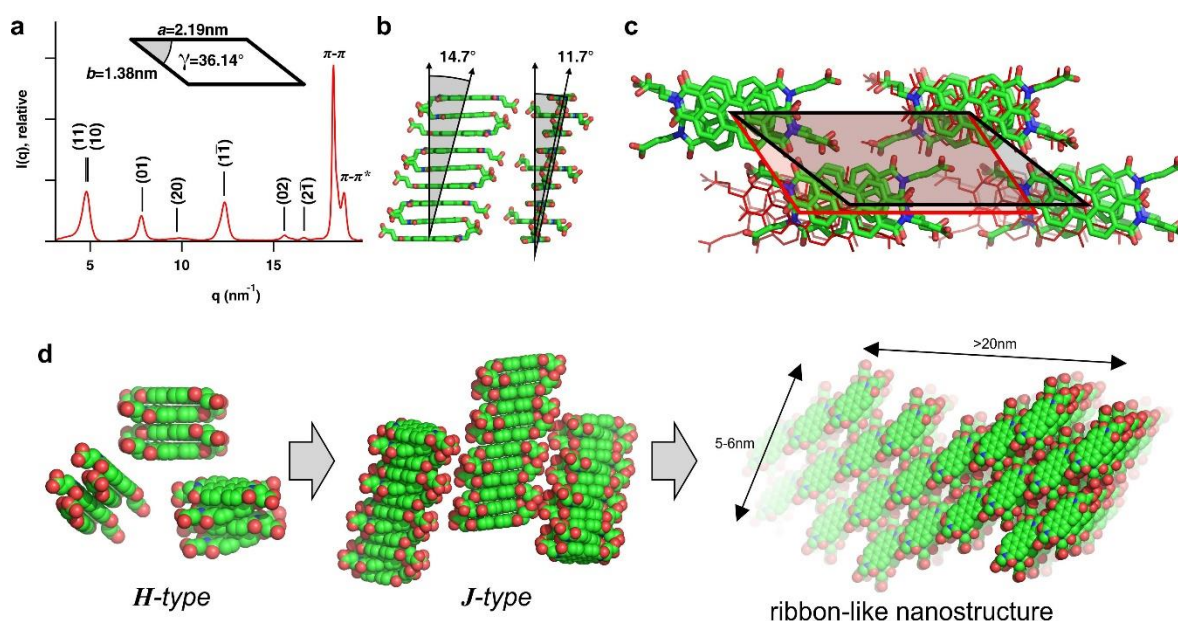

Figure 2| Molecular architecture within the PBI hydrogel. a, XRD pattern of the wet hydrogel. The sharp peaks correspond to the oblique unit cell (black inset) of π-π-stacked **PBI**. **b**, Lateral view of isolated π-π-stacked **PBI** columns. **c**, Top view of the unit cell within the hydrogel (black) compared to the single-crystalline motif (red). **d**, Schematic representation of the gelation process, starting from **H**-type tetramer-stacks in the precursor and resulting in **J**-type crystalline nano-ribbons acting as a structural backbone of the hydrogel.

Structural model. The comparison of the crystal- and hydrogel-scattering implies that only the intra-columnar motif previously found in the single-crystal is preserved in the gel state. This, in accord with the optical absorption measurements, confirms the presence of *J*-type stacked columns. Consequently, the oblique unit cell dimensions previously determined by single-crystal diffraction must relate to mean distances between the π-π-stacked columns. We took advantage of this circumstance and used a single molecular column from the crystallographic structure to build the model.

By doing so, the columnar cross-section only fits inside the hydrogel unit cell if both long axis are aligned parallel. The full structural arrangement then becomes apparent by multiplying the unit cell using its oblique dimensions. The resulting model compared to the single-crystalline structure is shown in Fig. 2c. The structural motif is similar in both cases: the columns appear to cross-link preferentially between the now protonated carboxylic groups. Yet, the distance along this direction is identical, which leaves polar channels for water to penetrate. However, the oblique unit cell angle decreases from 54.78° to 36.14°, resulting in a linear alignment of neighbouring lateral imide groups. Infrared spectra confirm this hypothesis: the peaks related to both the carboxylic and amidic C=O distances red-shift due to increasing peripheral interaction, such as hydrogen bonding (Supplementary Fig. 9). This strongly suggests hydrogen bonding between these moieties instead of electrostatic repulsion between the carbonyl oxygen atoms. Hence, the hydrogel comprises **PBI1** nano-ribbons with high crystalline order. A crucial side effect of this crystallinity is that the nano-ribbons are encapsulated by the carboxylic chains. These chains cross-link via hydrogen bonds and are therefore responsible for the structural cohesion between nano-ribbons.

Electrochemistry. To probe the accessibility of the imide groups and to derive additional information of the nano-ribbons' inner structure, we performed CO_2 absorption measurements. A variety of organic pigments including imides have been shown to absorb CO_2 at carbonyl

positions to form semicarbonates[34, 35, 36, 37, 38]. This phenomenon is directly seen in the redox properties of the pigments and can therefore be probed by cyclic voltammetry (CV) [34, 35, 36, 38]. A CV of the precursor **PBI1** in by N_2 flux deaerated aqueous solution shows two reduction processes centred around –0.3 and –0.7 V vs. Ag/AgCl, which correlate to the reduction of the carbonyl moieties (Fig. 3a). This redox activity disappears after purging the solution for 10 min with CO_2, which indicates the formation of the related semi-carbonate. The latter is not electrochemically active in the potential window between 0.2 and –0.8V. The same measurements obtained of the hydrogel yield a strikingly different result (Fig. 3b). The voltammograms are unaffected by the presence of CO_2 and show both under N_2 and CO_2 atmosphere a reversible redox couple centred around -0.3 V. This indicates that the imide groups are blocked by the close, intermolecular arrangement within the crystalline nano-ribbons, such that CO_2 cannot access the absorbing atomic sites. This effect emphasizes the importance of the structure-function interplay and further corroborates the molecular model of the hydrogel in Fig. 2c and d.
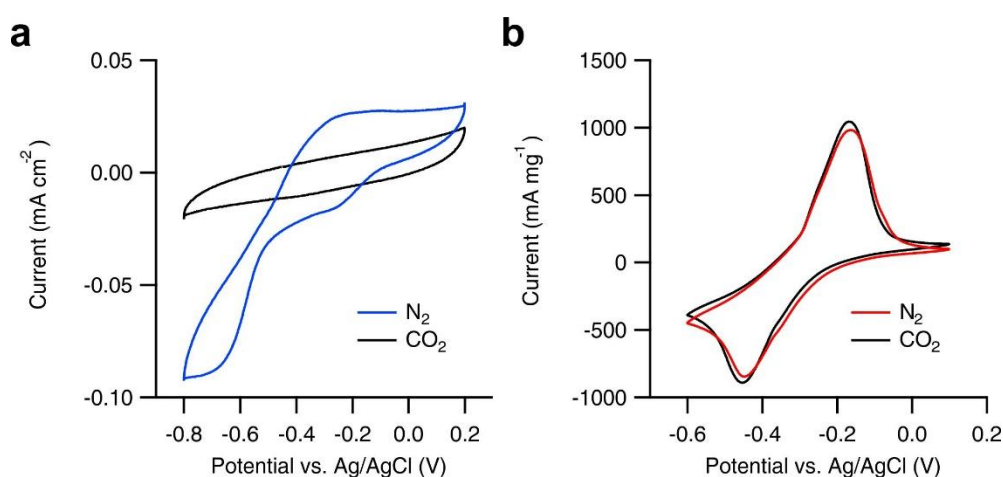

Figure 3| CO_2 absorption by the PBI1 and the hydrogel. a, Cyclic voltammograms of the **PBI1** precursor solution when N_2 purged (blue) and after 10 min purging with CO_2 (black) at a glassy carbon working electrode. **b**, Cyclic voltammograms of the immobilized hydrogel under N_2 (red) and CO_2 atmosphere (black). All measurements were recorded at 50 mV s^{-1}.

Inter-ribbon charge transfer. The crystalline nature of the nano-ribbons is of particular importance for long-range charge-transfer as it enables charge-mobility along the π-π-stacked columns[39, 40]. However, this mechanism is only one-dimensional. Bulk-conductivity over all three dimensions therefore requires charge transfer along the *lateral* directions, that is between the π-π-stacked columns and further between the crystalline nano-ribbons. As both of these structural features, the π-π-stacked columns as well as the crystalline nano-ribbons, are inter-connected via hydrogen-bonding, charge-transfer between two entities must occur via such bridging sites. If this hypothesis is correct, the choice of medium either activates or de-activates the hydrogen-bridging sites and therefore long-range charge-transfer. Bulk conductivity in turn can therefore be used to probe the surrounding medium – a prerequisite for gas-sensing materials.

To investigate these *lateral* inter-columnar charge transfer mechanisms, we fabricated simple gas-sensing devices by drop-casting a **PBI1** hydrogel film between two Au electrodes on a glass substrate as detailed in the Methods. The electrode spacing of 300 μm is unlikely to be bridged by a single hydrogel ribbon and thus this setup measures overall bulk-conduction including inter-backbone conduction. SEM images and grazing incidence SAXS (GISAXS) measurements confirm that the hydrogel-characteristic nano-ribbons as well as the intermolecular motif remain intact after drying, (Fig. 4a and Supplementary Figs. 10 and 11). In a dry state, the current through the hydrogel is as low as 2 pA at a bias of 2 V. When the sample is repeatedly exposed to 300 ms pulses of H_2O saturated air using a custom gas-flow setup (see illustration in Fig. 4a), the current increased by nearly five orders of magnitude to 93.3±3.3 nA (Fig. 4b). We probed the response time to humidity changes using 100 ms pulses, which led to a sharp rise in current within 10s of ms and re-equilibration to the dry conditions within two seconds (Fig. 4c).

We attribute this behaviour to the solvent-induced activation of the *lateral* inter-columnar charge transfer. We stipulate that the previously determined carboxylic groups are not only responsible for the structural cohesion but also act as conduction bridges between nano-ribbons. Water forms temporary hydrogen bridges between the nano-ribbons, allowing for charge transfer between them. Upon flushing the sample with N_2, the intercalated water is removed such that conduction between the nano-ribbons is suppressed.
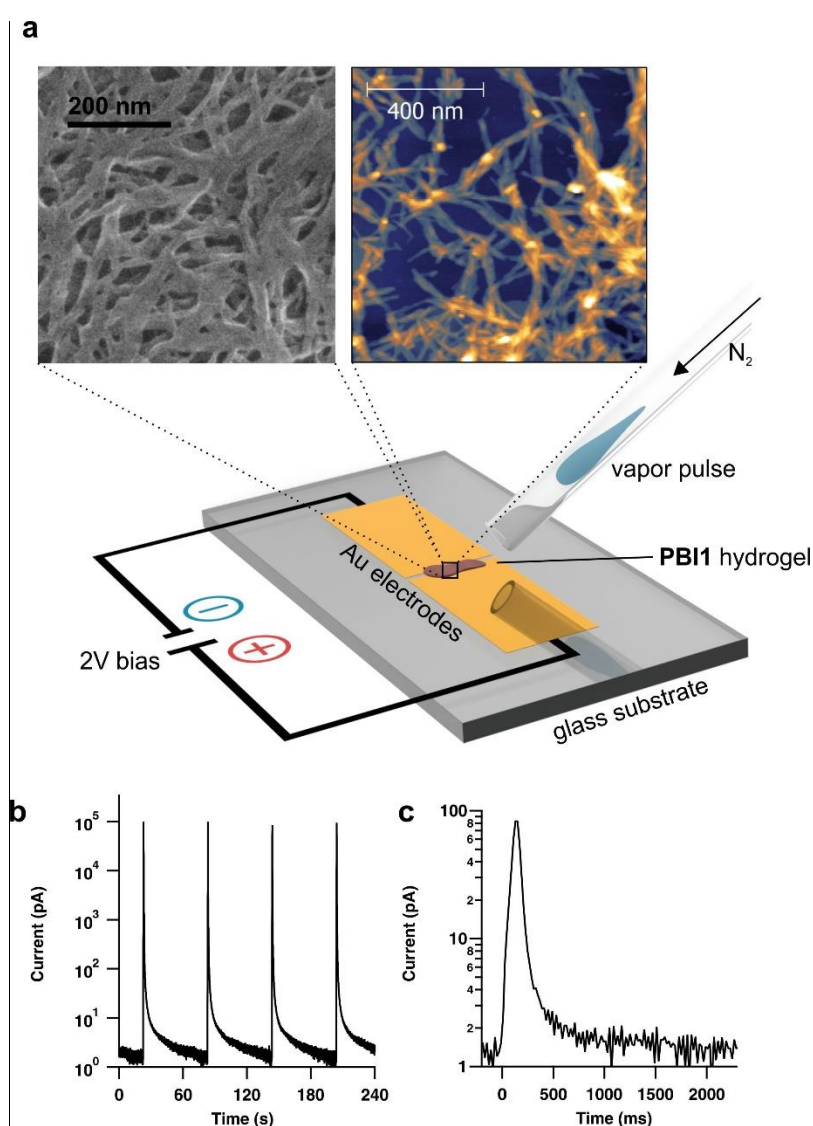

Figure 4| Electric response of the dried hydrogel to polar vapor. a, Schematic representation of the experimental setup together with AFM and SEM image of the dried hydrogel, confirming the ribbon-like nature of the hydrogel also in the dried state. **b**, Electrical response after deposition of 300 ms pulses of saturated H_2O

vapor, showing an increase of conductivity over 5 orders of magnitude. **c**, Time-resolved electrical response of a single 100 ms pulse of saturated H_2O.

DISCUSSION

Synthetic routes and theoretical calculations of amphiphilic perylene imide hydrogels are known in literature[23, 41, 42]. Despite the large number of works that appeared in the field of perylene bisimides gels[43, 44, 45], only few examples presented hydrogels[16, 21, 46, 47] and fewer provide experimental insights into the hydrogels' structure[5, 16, 48]. Here, we present a structural model for perylene imide based hydrogels, in particular the basic derivative β-alanine functionalized perylene bisimide **PBI1**.

Datar et al. suggested hydrogen bonding between adjacent carboxylic groups to be responsible for the gel-like nature of the hydrogel[41]. By combining scattering, microscopic, electrochemical, and electrical methods we could, however, construct a comprehensive structural model based on a hierarchy of structure directing motifs. First, π-π-stacking is without doubt the characteristic structural motif to form **PBI1** columns. Second, the protonated carboxylic groups of **PBI1** are responsible for longitudinal cross-linking between the π-π-stacked columns. Third, from the X-ray scattering data we find the symmetric imide groups to be responsible for the lateral *in-plane* attachment between the π-π-stacked columns (Figure 2c). We find confirmation for this structure in the CO_2 absorption measurements; while accessible in the precursor the imide positions are structurally blocked in the hydrogel, such that CO_2 cannot access the carbonyl groups and cannot be absorbed. The X-ray scattering data provides further support for this arrangement of the π-π-stacked columns within the nano-ribbons since other arrangements would result in different diffraction-peaks for the unit-cell family.

This detailed structural picture allows to understand, e.g., charge-transfer phenomena as a prominent feature of the hydrogel. We have shown that the nano-ribbon surface is mostly defined by dangling carboxylic groups looking to cross-link with neighbouring sites. This cross-

linking is responsible for the structural cohesion of the gel in aqueous media and provides mechanical deformability. It is also very likely that inter-ribbon charge-transfer occurs along these bonding sites, as only here the structural vicinity for charge-hopping is given. Hence, carboxylic groups of adjacent nano-ribbons form conduction bridges, responsible for the structural *and* electronic properties of the overall hydrogel.

We probed and used the cross-linking by measuring the dried hydrogel response to polar vapour. Short water vapour pulses directed onto the dry hydrogel activate conduction bridges between the nano-ribbons as seen by a fast conductivity increase of almost five orders of magnitude. Upon re-drying of the gel with N_2 these bridges are broken up and long-range charge-transfer is impeded.

In conclusion, we reconstructed the structural motif of a pH triggered perylenebisimide (PBI) hydrogel from scattering data and complementary methods and could derive an understanding of the charge-transfer mechanisms within the gel. We draw a precise structure-function correlation dominated by the electronegative carbonyl sites of the PBI. These groups are not only responsible for the mechanical properties of the gel, but also enable long-range charge-transfer within the gel's inner skeleton. The underlying conduction bridges can be passivated and reactivated by consecutive drying and exposure to polar solvent vapour – a working principle for gas-sensing applications.

METHODS

Small and wide angle x-ray scattering

SAXS measurements Small angle x-ray scattering (SAXS) measurements were performed at the Austrian SAXS beamline of the electron storage ring ELETTRA using a photon energy of 8 keV[49]. The beamline setup was adjusted to a sample to detector distance of 760 mm to result in an accessible q-range 0.12–9 nm^{-1}. All images were recorded using the Pilatus 1M detector (Dectris, Switzerland) with at least 5 exposures of 20 seconds per sample to check for radiation damage. Reference patterns to calibrate the q-scale were collected of silver-behenate (*d*-spacings of 5.838 nm). All measurements were done using a 1.5 mm quartz flow cell capillary. The radial averaging and the image calibration were conducted using the FIT2D software[50]. All presented data was corrected for fluctuations of the primary intensity and the corresponding background has been subtracted from each solution scattering pattern.

Electrochemical measurements

The electrochemical measurements were performed by means of cyclic voltammetry, employing a standard three-electrode setup in an air-tight glass cells with separate gas inlet and outlet through an oil-filled bubbler. In all cases, Pt and Ag/AgCl were used as counter and reference electrode, respectively. The voltammograms were recorded with a constant scan rate of 50 mV s^{-1}. In case of the precursor measurements, 1 mL precursor solution was mixed with in 3 mL 0.1 M $NaSO_4$ and a 3 mm diameter glassy carbon was used as working electrode. In case of the hydrogel, the working electrode was made by immobilizing 250 μl of the final hydrogel between two pieces of carbon paper (Freudenberg, H2315). 0.1M $NaSO_4$ was equally used as electrolyte. The cell was either purged with N_2 or CO_2.

Vapour response measurements

We carried out vapour-response measurements using a custom-built humidity setup. Substrates were prepared by deposition of 40 nm Au on 15 nm Cr electrodes onto glass (previously cleaned

in piranha solution) under clean-room conditions. The effective distance between the electrodes was 300μm. After cleaning the substrates with isopropanol, 100 µl of the final gel were drop-casted between the electrodes and dried for 2 hours under N_2 atmosphere. During the measurement, samples were kept under continuous N_2 flow (2 L/min). Vapour pulses were generated using a function generator (Highland P400) controlling gas-flow valves to briefly redirect the N_2 flow into a container with saturated solvent vapour such that only small vapour pulses arrive directly at the sample. All measurements were conducted at both +2 and –2V to ensure repeatability and avoid possible mass-transport effects. The current was measured using a 4-probe setup directly placed on the Au electrodes (Agilent B1500 Semiconductor Device Analyser).

REFERENCES

1.   Würthner F, Saha-Möller CR, Fimmel B, Ogi S, Leowanawat P, Schmidt D. Perylene Bisimide Dye Assemblies as Archetype Functional Supramolecular Materials. *Chem Rev* **116**, 962-1052 (2016).

2.   Huang C, Barlow S, Marder SR. Perylene-3,4,9,10-tetracarboxylic Acid Diimides: Synthesis, Physical Properties, and Use in Organic Electronics. *J Org Chem* **76**, 2386-2407 (2011).

3.   Chen S, Slattum P, Wang C, Zang L. Self-Assembly of Perylene Imide Molecules into 1D Nanostructures: Methods, Morphologies, and Applications. *Chem Rev*, (2015).

4.   Görl D, Zhang X, Würthner F. Molecular Assemblies of Perylene Bisimide Dyes in Water. *Angew Chem Int Ed* **51**, 6328-6348 (2012).

5.   Weingarten AS, *et al.* Self-assembling hydrogel scaffolds for photocatalytic hydrogen production. *Nat Chem* **6**, 964-970 (2014).

6.   Wang Q, *et al.* Supramolecular aggregates as sensory ensembles. *Chem Commun* **52**, 12929-12939 (2016).

7.   Pfattner R, *et al.* Photo-induced intramolecular charge transfer in an ambipolar field-effect transistor based on a [small pi]-conjugated donor-acceptor dyad. *J Mater Chem C* **1**, 3985-3988 (2013).

8.   Erten-Ela S, Turkmen G. Perylene imide dyes for solid-state dye-sensitized solar cells: Spectroscopy, energy levels and photovoltaic performance. *Renewable Energy* **36**, 1821-1825 (2011).

9.   Li C, Wonneberger H. Perylene Imides for Organic Photovoltaics: Yesterday, Today, and Tomorrow. *Adv Mater* **24**, 613-636 (2012).

10.   Hestand NJ, Spano FC. Molecular Aggregate Photophysics beyond the Kasha Model: Novel Design Principles for Organic Materials. *Acc Chem Res* **50**, 341-350 (2017).

11.   Whitesides GM, Boncheva M. Beyond molecules: Self-assembly of mesoscopic and macroscopic components. *Proc Natl Acad Sci USA* **99**, 4769-4774 (2002).

12.   Chen Z, *et al.* Photoluminescence and Conductivity of Self-Assembled π–π Stacks of Perylene Bisimide Dyes. *Chem Eur J* **13**, 436-449 (2007).

13. Ferlauto L*, et al.* Enhancing the Charge Transport in Solution-Processed Perylene Di-imide Transistors via Thermal Annealing of Metastable Disordered Films. *Adv Funct Mater* **24**, 5503-5510 (2014).

14. Voorhaar L, Hoogenboom R. Supramolecular polymer networks: hydrogels and bulk materials. *Chem Soc Rev* **45**, 4013-4031 (2016).

15. Du X, Zhou J, Shi J, Xu B. Supramolecular Hydrogelators and Hydrogels: From Soft Matter to Molecular Biomaterials. *Chem Rev* **115**, 13165-13307 (2015).

16. Gorl D, Soberats B, Herbst S, Stepanenko V, Wurthner F. Perylene bisimide hydrogels and lyotropic liquid crystals with temperature-responsive color change. *Chem Sci* **7**, 6786-6790 (2016).

17. Elisseeff J. Hydrogels: Structure starts to gel. *Nat Mater* **7**, 271-273 (2008).

18. Shi Y, Peng L, Yu G. Nanostructured conducting polymer hydrogels for energy storage applications. *Nanoscale* **7**, 12796-12806 (2015).

19. Erbas A, Olvera de la Cruz M. Energy Conversion in Polyelectrolyte Hydrogels. *ACS Macro Lett* **4**, 857-861 (2015).

20. Draper ER, Adams DJ. Low-Molecular-Weight Gels: The State of the Art. *Chem* **3**, 390-410.

21. Kularatne RS, Kim H, Ammanamanchi M, Hayenga HN, Ware TH. Shape-Morphing Chromonic Liquid Crystal Hydrogels. *Chem Mater* **28**, 8489-8492 (2016).

22. Draper ER*, et al.* Air-stable photoconductive films formed from perylene bisimide gelators. *J Mater Chem C* **2**, 5570-5575 (2014).

23. Draper ER, Greeves BJ, Barrow M, Schweins R, Zwijnenburg MA, Adams DJ. pH-Directed Aggregation to Control Photoconductivity in Self-Assembled Perylene Bisimides. *Chem* **2**, 716-731 (2017).

24. Draper ER*, et al.* Reversible Photoreduction as a Trigger for Photoresponsive Gels. *Chem Mater* **28**, 6336-6341 (2016).

25. Rigodanza F, Tenori E, Bonasera A, Syrgiannis Z, Prato M. Fast and Efficient Microwave-Assisted Synthesis of Perylenebisimides. *Eur J Org Chem* **2015**, 5060-5063 (2015).

26. Zhang X, Görl D, Stepanenko V, Würthner F. Hierarchical Growth of Fluorescent Dye Aggregates in Water by Fusion of Segmented Nanostructures. *Angew Chem Int Ed* **53**, 1270-1274 (2014).

27. Shao C, Grüne M, Stolte M, Würthner F. Perylene Bisimide Dimer Aggregates: Fundamental Insights into Self-Assembly by NMR and UV/Vis Spectroscopy. *Chem Eur J* **18**, 13665-13677 (2012).

28. Ghosh S, Li X-Q, Stepanenko V, Würthner F. Control of H- and J-Type π Stacking by Peripheral Alkyl Chains and Self-Sorting Phenomena in Perylene Bisimide Homo- and Heteroaggregates. *Chem Eur J* **14**, 11343-11357 (2008).

29. Chen Z, Lohr A, Saha-Moller CR, Wurthner F. Self-assembled [small pi]-stacks of functional dyes in solution: structural and thermodynamic features. *Chem Soc Rev* **38**, 564-584 (2009).

30. Lim JM, *et al.* Exciton delocalization and dynamics in helical [small pi]-stacks of self-assembled perylene bisimides. *Chem Sci* **4**, 388-397 (2013).

31. Yagai S, Seki T, Karatsu T, Kitamura A, Würthner F. Transformation from H- to J-Aggregated Perylene Bisimide Dyes by Complexation with Cyanurates. *Angew Chem Int Ed* **47**, 3367-3371 (2008).

32. Kaiser TE, Stepanenko V, Würthner F. Fluorescent J-Aggregates of Core-Substituted Perylene Bisimides: Studies on Structure−Property Relationship, Nucleation−Elongation Mechanism, and Sergeants-and-Soldiers Principle. *J Am Chem Soc* **131**, 6719-6732 (2009).

33. Glatter O, Kratky O. *Small Angle X-ray Scattering*. Academic Press (1982).

34. Weinberg NL, Kentaro Hoffmann A, Reddy TB. The electrochemical reductive carboxylation of benzalaniline in molten tetraethyl ammonium p-toluenesulfonate. *Tetrahedron Lett* **12**, 2271-2274 (1971).

35. Apaydin DH, Głowacki ED, Portenkirchner E, Sariciftci NS. Direct Electrochemical Capture and Release of Carbon Dioxide Using an Industrial Organic Pigment: Quinacridone. *Angew Chem Int Ed* **53**, 6819-6822 (2014).

36. Singh P, Rheinhardt JH, Olson JZ, Tarakeshwar P, Mujica V, Buttry DA. Electrochemical Capture and Release of Carbon Dioxide Using a Disulfide–Thiocarbonate Redox Cycle. *J Am Chem Soc* **139**, 1033-1036 (2017).

37. Apaydin DH, *et al.* Electrochemical Capture and Release of CO_2 in Aqueous Electrolytes Using an Organic Semiconductor Electrode. *ACS Appl Mater Interfaces* **9**, 12919-12923 (2017).

38. Rheinhardt JH, Singh P, Tarakeshwar P, Buttry DA. Electrochemical Capture and Release of Carbon Dioxide. *ACS Energy Letters* **2**, 454-461 (2017).

39. Wu N, Wang C, Slattum PM, Zhang Y, Yang X, Zang L. Persistent Photoconductivity in Perylene Diimide Nanofiber Materials. *ACS Energy Lett* **1**, 906-912 (2016).

40. Fink RF, *et al.* Exciton Trapping in π-Conjugated Materials: A Quantum-Chemistry-Based Protocol Applied to Perylene Bisimide Dye Aggregates. *J Am Chem Soc* **130**, 12858-12859 (2008).

41. Datar A, Balakrishnan K, Zang L. One-dimensional self-assembly of a water soluble perylene diimide molecule by pH triggered hydrogelation. *Chem Commun* **49**, 6894-6896 (2013).

42. Roy S, Kumar Maiti D, Panigrahi S, Basak D, Banerjee A. A new hydrogel from an amino acid-based perylene bisimide and its semiconducting, photo-switching behaviour. *RSC Advances* **2**, 11053-11060 (2012).

43. Krieg E, *et al.* Supramolecular Gel Based on a Perylene Diimide Dye: Multiple Stimuli Responsiveness, Robustness, and Photofunction. *J Am Chem Soc* **131**, 14365-14373 (2009).

44. Roy S, Maiti DK, Panigrahi S, Basak D, Banerjee A. A bolaamphiphilic amino acid appended photo-switching supramolecular gel and tuning of photo-switching behaviour. *Physical Chemistry Chemical Physics* **16**, 6041-6049 (2014).

45. Wang A, *et al.* Tuning Supramolecular Structure and Functions of Peptide bola-Amphiphile by Solvent Evaporation–Dissolution. *ACS Appl Mater Interfaces* **9**, 21390-21396 (2017).

46. Weingarten AS, Kazantsev RV, Palmer LC, Fairfield DJ, Koltonow AR, Stupp SI. Supramolecular Packing Controls H2 Photocatalysis in Chromophore Amphiphile Hydrogels. *J Am Chem Soc* **137**, 15241-15246 (2015).

47.   Castilla AM, *et al.* Self-sorted Oligophenylvinylene and Perylene Bisimide Hydrogels. *Scientific Reports* **7**, 8380 (2017).

48.   Sukul PK, Singh PK, Maji SK, Malik S. Aggregation induced chirality in a self assembled perylene based hydrogel: application of the intracellular pH measurement. *Journal of Materials Chemistry B* **1**, 153-156 (2013).

49.   Amenitsch H, Rappolt M, Kriechbaum M, Mio H, Laggner P, Bernstorff S. First performance assessment of the small-angle X-ray scattering beamline at ELETTRA. *Journal of synchrotron radiation* **5**, 506-508 (1998).

50.   Hammersley AP, Svensson SO, Thompson A, Graafsma H, Kvick Å, J P Moy. Calibration and correction of distortions in 2D detector systems. *Rev Sci Instr* **66**, 4 (1995).

ACKNOWLEDGEMENTS

AUTHOR CONTRIBUTIONS

M.B. and F.R. contributed equally to this work. F.R. and Z.S. prepared and synthesized samples, M.B., F.R., H.A. and Z.S. performed SAXS, GISAXS and WAXS experiments, M.B. grew PBI single-crystals, N.D. conducted single-crystal XRD and reconstructed the crystal-structure, S. M. conducted rheometry and DSC experiments, T.S. and M.B. conducted humidity response measurements, I.L. obtained CryoTEM images, I.K. obtained SEM and AFM images of drop-casted and dried samples, Z.S. obtained AFM images of spin-coated samples, M.B., E.M. and S.A.F. conducted CO_2 absorption CV measurements, H.A., M.P. and Z.S planned and supervised the research. All authors contributed to writing the manuscript.

COMPETING INTERESTS

The authors declare no competing interests.